Journal of Inflammation Research

Dovepress
Taylor & Francis Group

Open Access Full Text Article

ORIGINAL RESEARCH

Neutrophil-Specific Biomarker S100A2 Mediates Diabetic Foot Ulcer Through IL-17 Signaling Pathway and Potential Therapeutics

Luqin Lv[1,2,*], Yizhuo Zhang[1,2,*], Xiaoming Zhu[3], Qiaoli Cui[3], Yijian Chen[1,2]

[1]Institute of Antibiotics, Huashan Hospital, Fudan University, Shanghai, People's Republic of China; [2]Key Laboratory of Clinical Pharmacology of Antibiotics, National Health Commission, Shanghai, People's Republic of China; [3]Department of Endocrinology, Huashan Hospital, Fudan University, Shanghai, People's Republic of China

*These authors contributed equally to this work

Correspondence: Yijian Chen, Email chenyijian@fudan.edu.cn

Background: Diabetic foot ulcers (DFU) often lead to infection and amputation, thereby imposing a heavy socioeconomic burden. The limited efficacy of current therapies underscores the urgent need to explore the pathogenesis of DFU. Alterations in the immune response have been reported to influence the pathophysiology of DFU by single-cell RNA sequencing (scRNA-seq) analysis. Therefore, a thorough understanding of the immune microenvironment characteristics of DFU and the intervention of specific immune cell populations could enable the formulation of optimal therapeutic strategies.

Methods: Bulk RNA sequencing (bulk RNA-seq) datasets and scRNA-seq datasets were acquired from the Gene Expression Omnibus (GEO) database. The packages "limma", "weighted gene coexpression network analysis (WGCNA)", and "CIBERSORT" were used for bulk RNA-seq analysis to identify the key immune genes. For scRNA-seq, the packages "Seurat" were used for cell clusters identification and annotation. The differential expression of immune hub genes between DFU and diabetic foot skin (DFS) was validated using quantitative real-time polymerase chain reaction (qRT-PCR) and our RNA-seq dataset. A Connectivity Map (CMAP) database was used for computational drug prediction.

Results: Using bulk-RNA-seq, seven genes were identified as immune hub genes. Afterwards, six cell populations were recognized by scRNA-seq, with S100A2 predominantly expressed in neutrophils. Moreover, we revealed a robust correlation between the interleukin-17 (IL-17) signaling pathway and S100A2. Secukinumab, ruxolitinib, and leflunomide are potential therapeutic drugs for DFU. Among them, ruxolitinib and leflunomide are clinically available agents, while secukinumab (an IL-17A inhibitor) shows translational potential for repurposing.

Conclusion: S100A2 appears to be a promising therapeutic target for the modulation of DFU pathogenesis. Furthermore, neutrophil-mediated inflammatory responses and immune regulation appear to be crucial factors in DFU progression. Notably, this is the first study to identify S100A2 as a neutrophil-specific biomarker linked to IL-17 signaling in DFU, filling the gap of specific gene-immune cell interaction in DFU pathogenesis.

Keywords: diabetic foot ulcer, single-cell RNA sequencing, immune infiltration, IL-17 signaling pathway, drug prediction

Introduction

According to data from the World Health Organization, 422 million people have diabetes[1] with up to 25% developing diabetic foot ulcer (DFU) during disease progression.[2] DFU is among the most prevalent diabetes-related lower extremity complications (DRLECs).[3] DFU cases frequently progress to infection and approximately 20% of amputations, representing the leading cause of morbidity and mortality.[4] Furthermore, DFU management imposes an increasing socioeconomic burden, estimated at $9–13 billion annually in the United State.[5] Neuropathy, peripheral artery disease, and chronic hyperglycemia significantly influence wound development.[6] Wound healing progresses through four distinct but overlapping phases: hemostasis, inflammation, proliferation, and remodeling. These phases require coordinated interactions between various

https://doi.org/10.2147/JIR.S577432
Received: 18 November 2025
Accepted: 11 March 2026
Published: 23 March 2026

cells, extracellular components, growth factors, and cytokines.[7] Recent decades have witnessed emerging research on molecular mediators, such as nitric oxide (NO), exosomes, TGF-β, colony-stimulating factors (CSFs), and matrix metalloproteinases (MMPs) in diabetic foot,[8] the cellular mechanisms underlying DFU pathogenesis remain poorly characterized. Although DFU-associated costs are reduced by current treatments, such as glycemic management, wound debridement and dressings, preventive measures, patient and staff training, multidisciplinary therapy, and intense monitoring, clinical outcomes remain far from satisfactory.[9,10] Systematic clarification of the molecular underpinnings of DFU development is imperative to advance precision medical approaches and potentially provide novel opportunities for therapies and prevention.

RNA high-throughput sequencing has become a cornerstone technique in biological research, facilitating the discovery of immune genes and distinction of immune cell heterogeneity. Georgios et al[11] conclude that DFU pathogenesis is driven by dysregulated immune responses in which immune cell activation, proliferation, and survival are based on single-cell RNA sequencing (scRNA-seq) revealed a signature immune cell profile with impaired macrophage and neutrophil activation and proliferation. However, their study did not precisely elucidate the relationship between specific gene targets and the immune microenvironment, leaving a gap in understanding how to translate immune cell insights into targeted therapeutic strategies. Beyond this, prior transcriptomic studies of DFU have largely focused on documenting immune cell heterogeneity,[11] but few have identified neutrophil-specific biomarkers or their associated signaling pathways. Similarly, while S100A family proteins are well-established regulators of inflammation in skin conditions like psoriasis,[12,13] their functional role in DFU remains entirely uncharacterized. To address these interconnected gaps, our study systematically investigated immune hub genes in DFU through a multi-layered approach: we first identified key candidate genes via bulk RNA-seq analyses (encompassing differential expression, weighted gene coexpression network analysis (WGCNA), and immune infiltration assessments), then mapped their cellular expression patterns using scRNA-seq, and finally validated these findings via quantitative real-time polymerase chain reaction (qRT-PCR). By integrating bulk and single-cell sequencing data, we specifically linked the S100A2 protein to the IL-17 signaling pathway uncovering a novel mechanistic axis underlying DFU progression.

Additionally, given that nearly 50% of DFU patients develop secondary foot infections,[14] we also predicted potentially effective antibiotics to inform empirical treatment decisions for diabetic foot infections, adding a practical clinical dimension to our mechanistic findings.

Materials and Methods

Datasets Selection

Open access microarray and sequencing datasets were retrieved from the Gene Expression Omnibus database (GEO, http://www.ncbi.nlm.nih.gov/geo) with a search strategy focused on studies comparing diabetic foot ulcer (DFU) tissues and diabetic foot skin (DFS) tissues without ulcers. Three eligible datasets were identified: GSE80178,[15] GSE134431,[16] and GSE165816.[11] GSE80178 (released in 2016, GPL16686 platform) included 21 samples, consisting of 8 DFS samples and 13 DFU samples. GSE134431 (released in 2019, GPL18573 platform) contained 12 samples, with 3 DFS samples and 6 DFU samples (3 additional samples were excluded as they did not meet the DFU/DFS grouping criteria). GSE165816 (submitted on January 29, 2021, updated on January 12, 2022, GPL24676 Illumina NovaSeq 6000 platform) originally comprised 54 samples from 10 non-diabetic controls and 17 diabetic patients (11 with DFU and 6 without DFU). For the present analysis, we specifically selected 22 tissue samples that matched the DFU/DFS comparison criteria: 8 DFS samples (from diabetic patients without DFU) and 14 DFU samples (including both healing and non-healing DFU foot skin tissues). Bulk RNA-seq analyses were performed on GSE80178 and GSE134431, while single-cell RNA-seq (scRNA-seq) analysis was conducted on the selected samples from GSE165816. A flowchart of the study design and sample selection process is presented in Figure 1.

Bulk RNA-Seq Data Processing

The GSE80178 was initially normalized using the "limma" package of R, followed by screening of differentially expressed genes (DEGs) with a filter of |log 2 (fold-change) (FC) | >1 and an adjusted $P < 0.05$. The analytical results were depicted using a heat map and volcano plot using the "pheatmap" package and the "ggplot2" package, respectively.

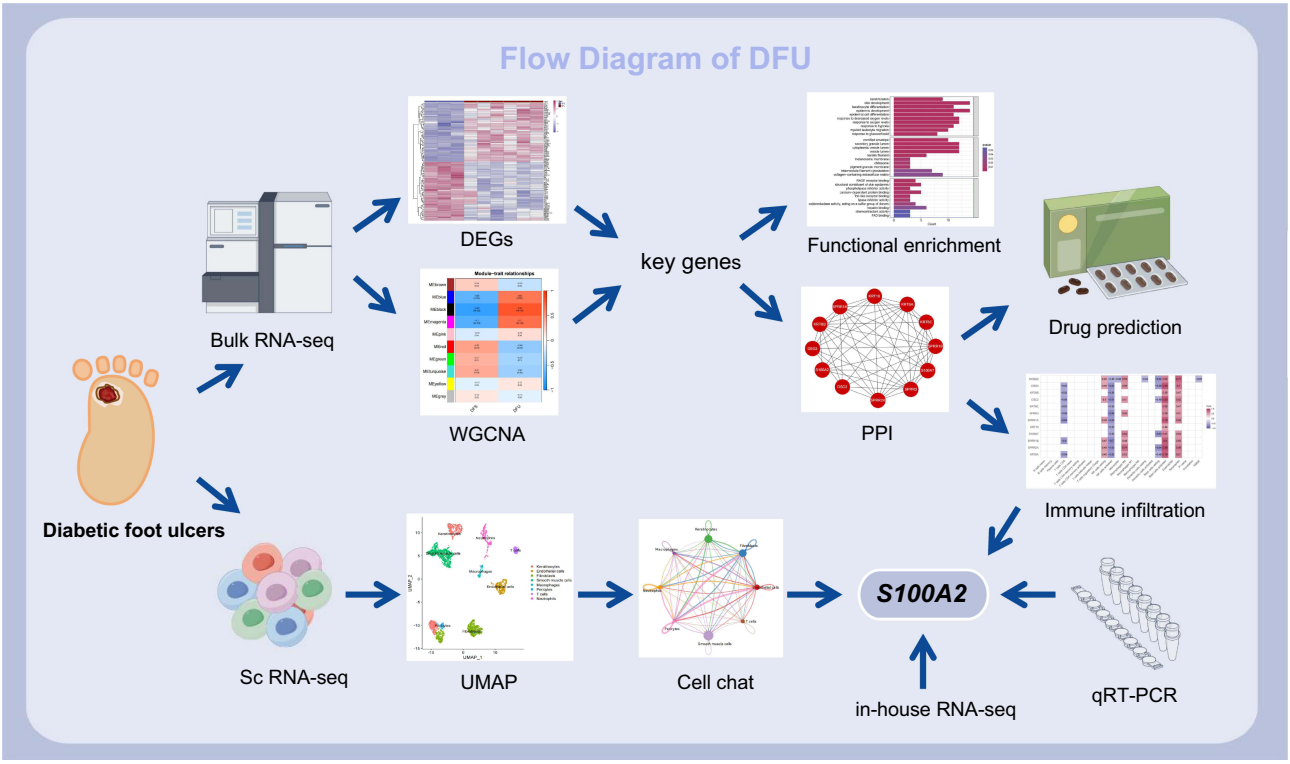

Figure 1 Study workflow.
Abbreviations: DFU, diabetic foot ulcer; DEGs, differentially expressed genes; PPI, protein-protein interaction; WGCNA, weighted gene coexpression network analysis (WGCNA); UMAP, uniform manifold approximation and projection.

GSE134431 was first normalized using the "limma" package and then constructed into a gene coexpression network by the "WGCNA" libraries. Initially, the gene expression data profiles were transformed into a similarity matrix based on the analogous expression patterns of all genes. Subsequently, this similarity matrix was converted into an adjacency matrix, which was further processed into a topological overlap matrix (TOM). Here, a power of 8 was ascertained via the pickSoftThreshold function of the WGCNA. Using average linkage hierarchical clustering, genes exhibiting homogeneous expression patterns were classified into distinct modules, adhering to a minimum cut-off value of 300. Module–trait correlations were evaluated by calculating the Pearson correlation coefficients between the gene modules and DFU status.

Significantly correlated modules were subjected to intersection analysis with DEGs via the "VennDiagram" package.

Comprehensive Analysis

To reveal the biological functions and signaling pathways of discovered key genes, gene ontology (GO) and Kyoto Encyclopedia of Genes and Genomes (KEGG) pathway enrichment were conducted using the "clusterProfiler" package under an adjusted $P < 0.05$. GO analysis covered three domains: enriched biological processes (BPs), molecular functions (MFs), and cellular components (CCs). Enriched terminologies were grouped according to membership similarity, with the most significantly enriched term chosen as representative.

To explore potential interactions among key genes, a protein-protein interaction (PPI) network was constructed using the Search Tool for the Retrieval of Interacting Genes (STRING) database (http://string-db.org/) with a cumulative score of interactions > 0.4. The top hub genes were identified using the Molecular Complex Detection (MCODE) plug of Cytoscape (v3.8.2).

Immunocyte Infiltration Analysis

The immunological infiltration patterns distinguishing DFU from DFS in GSE134431 were quantified using the CIBERSORT algorithm configured with the "PERM" parameter set to 1000 and a threshold of $P < 0.05$ anchored

https://doi.org/10.2147/JIR.S577432

to the identified hub genes. Subsequently, we performed multidimensional immunological profiling to deeply clarify the complex interplay among diabetic foot ulcer (DFU), immune cells, and hub genes. First, the immune cell composition was computed and is presented as a bar plot. The richness of infiltrating immune cells (22 subsets) was visualized via the "pheatmap" package and the content and differences of immune cells across DFS and DFU was shown by the "boxplot" package. The intercellular correlations were analyzed by the "corrplot" package.

Spearman analysis was performed to determine the relationship between immune cells and genes, using the "ggcorrplot" package. The following criteria were used to select key immune genes linked to DFU: correlation coefficient > 0.7 and $P < 0.05$.

Sc RNA-Seq Data Processing

Single-cell transcriptomic data were processed and analyzed using the "Seurat" libraries. Quality control was implemented based on the total number of expressed genes and mitochondrial gene content. Subsequently, normalization of the transcriptomic matrix was performed using log2 (CPM+1) transformation. Highly variable genes were detected through the "FindVariableGenes" function, followed by principal components (PCs) analysis. The number of PCs was modified to six to generate cell clusters with subsequent visualization and annotation via uniform manifold approximation and projection (UMAP). Additionally, the intercellular communication was analyzed with the "CellChat" package. Cell distribution and gene expression patterns were visualized using "DimPlot" and "FeaturePlot" functions, respectively. Then, Cluster-specific marker genes were identified through "FindAllMarkers" function and presented as a volcano map. Finally, the cell differentiation trajectory was inferred by "Monocle" package.

Validation on Clinical Samples

This study prospectively enrolled patients hospitalized at Huashan Hospital, Fudan University, between January 2023 and December 2024. DFU patients were included based on the following criteria: age 35–75 years, glycated hemoglobin (HbA1c) levels of 7–10%, ulcer severity classified as Wagner grade 2–5, normal white blood cell (WBC) count (4.0–10.0 $\times 10^3/\mu L$), and C-reactive protein (CRP) within the normal range (<10 mg/L). DFS patients were matched for age (35–75 years) and HbA1c (7–10%). The exclusion criteria were as follows: (1) non-diabetic ulcer (eg., venous or dermatopathy-induced ulcer), (2) recurrent DFU, (3) systemic comorbidities affecting wound healing (eg., malignancies, lupus erythematosus, cardiac/hepatic/renal failure), (4) history of lower-limb orthopedic surgery, (5) prior corticosteroid/immunosuppressive therapy (within 4 weeks), (6) ulcer above the ankle, and (7) pregnancy, lactation, or incomplete clinical data. The study protocol was approved by the Ethics Committee of Huashan Hospital, Fudan University (approval no. KY2016-395). Each participating patient provided written informed consent. Total mRNA was extracted from skin tissues using TRIzol reagent (Invitrogen, USA). RNA purity was evaluated using a NanoDrop 2000 spectrophotometer (Thermo Fisher Scientific). Subsequently, cDNA reverse transcription was performed using the PrimeScript RT Master Mix (Takara, Dalian, China). qRT-PCR experiments were performed using SuperReal PreMix Plus (Invitrogen) and QuantStudio Real-Time PCR Software (Thermo Fisher Scientific, USA). β-actin served as the endogenous control, and the primer sequences were as follows: forward primer F-TCACACAGCACTGGAGAAAGT and reverse primer R-AGAGTTCTGCTTCAGGGTCG. Quantitative assessment of relative expression was conducted using the $2^{(-\Delta\Delta Ct)}$ algorithm.

To further validate the reliability of our previous database analysis results, we conducted high-throughput sequencing of the aforementioned samples using Illumina Novaseq 6000, followed by a series of bioinformatics analyses.

Small Molecule Drugs Analysis

The Connectivity Map (CMAP) database contains the most extensive collection of transcriptomic profiles for drug interference therapies.[17] We queried 12 hub genes against CMAP and identified agents with negative connectivity scores as potential therapeutic candidates. Compounds were selected based on enrichment < −0.7 and $P < 0.01$.

Statistical Methodology

Numerical variables were described as mean ± standard deviation, and bioinformatics analyses were performed using R (v4.3.0; R Foundation for Statistical Computing, Vienna, Austria). To ensure the reliability and precision of the qPCR data, outliers in the DFU were identified and excluded using the Tukey's method. Sample sizes for clinical validation (6 DFS and 10 DFU samples) were determined based on the availability of qualified specimens meeting the inclusion/exclusion criteria and prior similar studies in the field. Batch effects in bulk RNA-seq were mitigated by WGCNA during co-expression module analysis, while technical biases were minimized by filtering low-quality cells (mitochondrial gene ratio <5%) in scRNA-seq and excluding outliers via Tukey's method in qRT-PCR. Intergroup comparisons were performed using unpaired two-tailed Student's t-tests in the GraphPad Prism software (v9.5.0; GraphPad Prism Software, San Diego, California, USA). $P < 0.05$ was set as the significance threshold.

Results

Key Genes Identification

The workflow of the gene screening is displayed in Figure 2. In GSE80178, both the heat map and volcano plot indicated the existence of 1790 DEGs, comprising upregulated 606 genes and 1184 downregulated genes (Figure 3A and B). In the GSE134431, initial sample clustering was executed with a threshold set at 80 (Figure 4A). Subsequently, a soft threshold power (β) of eight was chosen to construct a scale-free network with a truncated fitting index of $R^2 = 0.80$ (Figure 4B). Coexpression modules were detected, with each representing a gene with analogous expression patterns (Figure 4C). As reflected by the module-trait analyses, ten modules were related to DFU, among which the black module was the most significant (module feature correlation = 0. 83) (Figure 4D). A heatmap of the intermodular correlations is shown in Figure 4E. Notably, a strong correlation (r = 0.74) was observed between the 470 black module genes and the significance of DFU-related genes (Figure 4F).

In the Venn graph, 132 key genes were identified at the intersection of the DEGs and black module genes (Figure 5A).

Multifaceted Analysis of Key Genes

GO analysis demonstrated that these key genes were prominently enriched in BPs, including keratinization, skin development, and keratinocyte differentiation; MFs, including RAGE receptor binding, structural constituents of skin epidermis, phospholipase inhibitor activity; and CCs, including cornified envelope, secretory granule lumen, and cytoplasmic vesicle lumen (Figure 5B). KEGG pathway enrichment analysis revealed that these key genes were exclusively enriched in the interleukin-17 (IL-17) signaling pathway.

A PPI network was generated using the STRING database (Figure 5C) and the top 12 hub genes were screened based on degree centrality using the MCODE plugin in Cytoscape. These hub genes included KRT6A, SPRR2A, SPRR1B, S100A7, KRT16, SPRR1A, SPRR3, KRT6C, DSC2, KRT6B, DSG3, and S100A2 (Figure 5D).

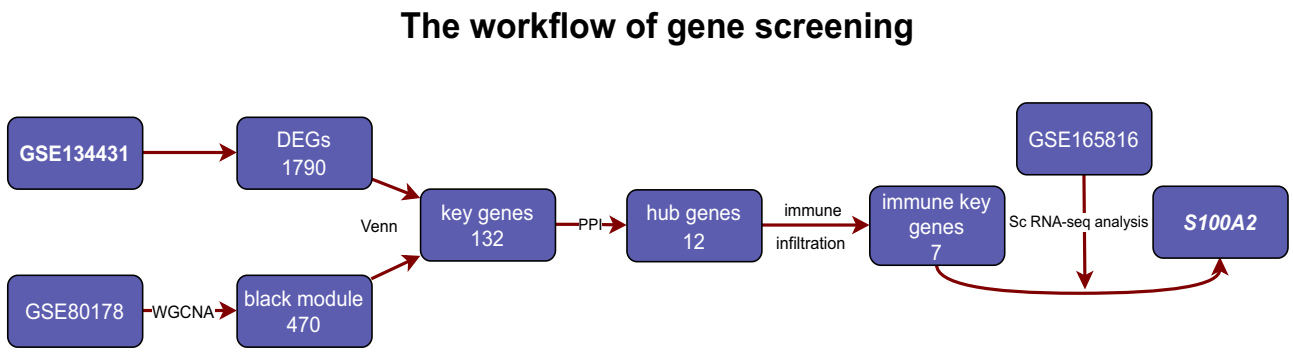

Figure 2 The workflow graph of gene selection.

https://doi.org/10.2147/JIR.S577432

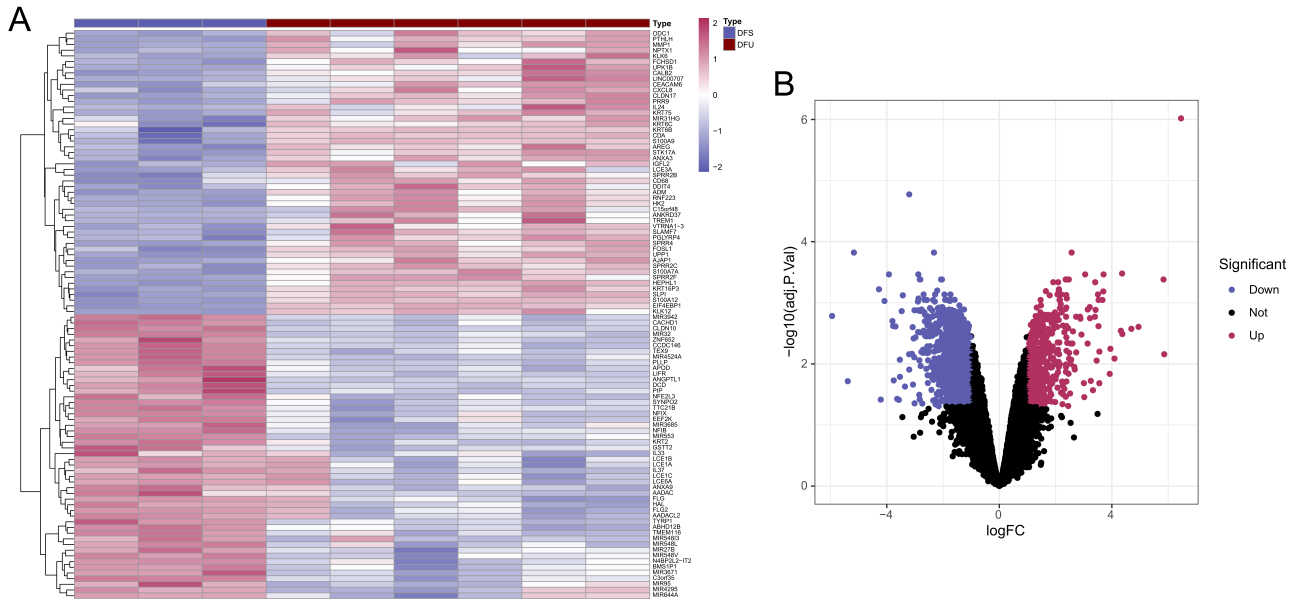

Figure 3 Detection of DEGs in the GSE80178. (**A**) Heat map of DEGs. (**B**) Volcano plot of DEGs.

Interactions Between Hub Genes and Immune Cells

Given the pivotal involvement of immune cell dynamics in DFU pathogenesis, we quantified the proportion and abundance of 22 immunocytes in the specimens using the CIBERSORT algorithm (Figure 6A and B). The levels of activated mast cells and neutrophils were higher in DFU than DFS, whereas the levels of activated NK cells and CD8+ T cells were lower (Figure 6C). We further investigated the correlation between different immune cells and 12 hub genes. Notably, CD8+ T cells exhibited the most robust positive correlation with T follicular helper cells (r = 0.97), whereas M0 macrophages showed the most profound negative correlation with resting NK cells (r = −0.94) (Figure 6D). By applying stringent screening criteria, seven genes (S100A2, DSG3, DSC2, SPRR1A, SPRR1B, KRT6A, and SPRR2A) were identified as the key immune genes (Figure 6E). Interestingly, S100A2 was the only protein with the strongest positive effect on neutrophils (Figure 6F).

Sc RNA-Seq Analysis and Cellular Characterization

In GSE165816, a quality control procedure was implemented by excluding low-quality cells and controlling mitochondrial and red blood cell gene content. After selecting highly variable genes, the dimensionality was reduced, and meaningful features were extracted. Subsequently, 8 cell subpopulations (smooth muscle cells, endothelial cells, fibroblasts, macrophages, T cells, neutrophils, pericytes, and keratinocyte subsets) were resolved in the UMAP plot (Figure 7A), covering the core functional populations involved in DFU wound healing. The number and strength of intercellular crosstalk between the 8 cell subsets are shown in Figure 7B. Among these interactions, neutrophils and macrophages exhibited prominent mutual crosstalk; meanwhile, both neutrophils and macrophages also showed strong interactions with fibroblasts, endothelial cells, and keratinocyte subsets. The expression patterns of key immune genes across clusters were visualized in the form of violin and UMAP plots, revealing pronounced S100A2 enrichment in neutrophils (Figure 7C and D). S100A2 served as a neutrophil-specific marker. Consistent with bulk RNA-seq findings, S100A2 was significantly upregulated in scRNA-seq (Figure 7E). Pseudotime trajectory analysis showed that neutrophils serve as the starting population of the trajectory, and then differentiate toward three distinct directions (Figure 7F). Lighter colors in the plot represent the terminal stage of differentiation, reflecting the dynamic cell state transitions of neutrophils during DFU progression.

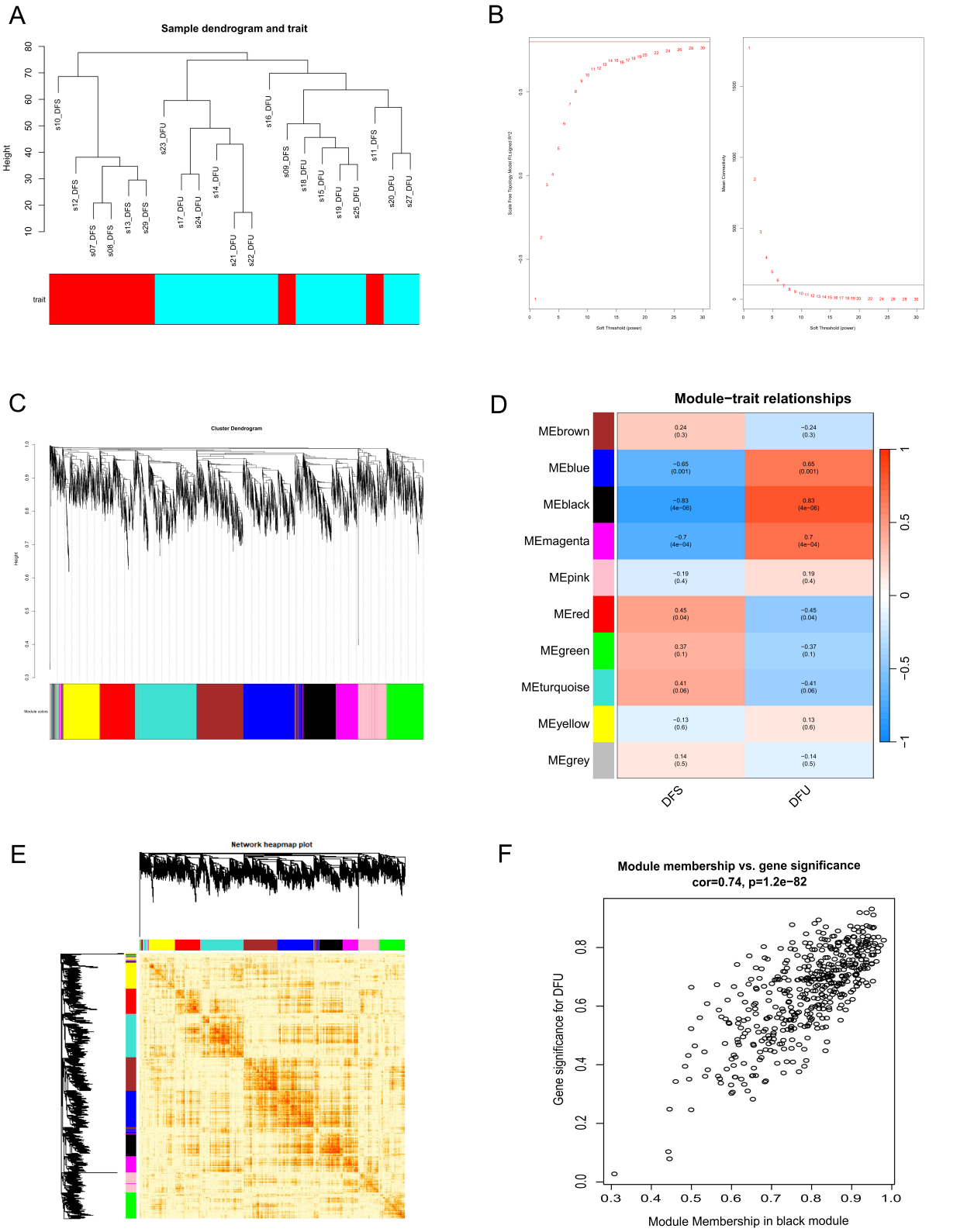

Figure 4 Identification of key modules genes in the GSE134431. (**A**) Dendrogram of sample clustering based on 21 samples' phenotypic traits. (**B**) Selection of optimal soft-threshold power (scale-free topology fit, R^2 = 0.80). (**C**) Coexpression module construction: genes were clustered by expression similarity and color-coded by module assignment. (**D**) Module-trait correlations. The black module was significantly correlated with DFU (COR = 0.83, $P < 0.001$) and DFS (COR = −0.83, $P < 0.001$). (**E**) Heat map of inter-modular correlations. (**F**) Correlation between the black module and DFU. Gene significance for DFU refers to compare the correlation between individual gene and its corresponding traits.

https://doi.org/10.2147/JIR.S577432

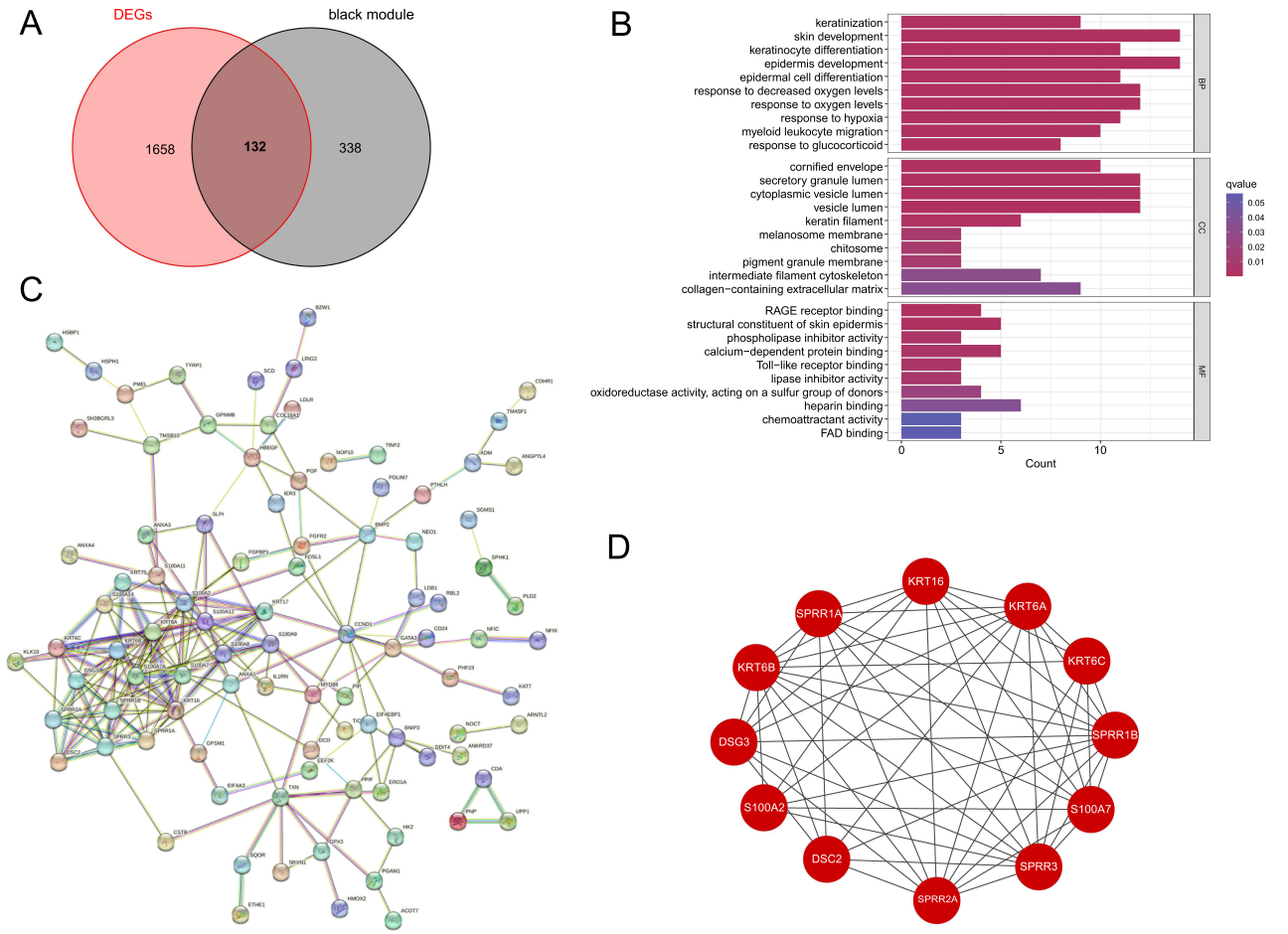

Figure 5 Integrated analysis of key genes. (**A**) Venn diagram: 134 overlapping genes between DEGs and black module genes. (**B**) Enrichment results of DEGs using Gene Ontology (GO). X-axis: the gene count in certain terms; Y-axis: the different items of functions. BP, biological process; CC, cellular component; MF, molecular function; (**C**) Protein-protein interaction (PPI) network of key genes. (**D**) 12 hub genes were classified in the PPI through the MCODE application.

Immune Hub Genes Validation

Tissue specimens (six DFS and 10 DFU) were obtained from 16 patients with diabetes. The relative expression of the immune hub genes was detected in the DFU and DFS groups. Figure 8 shows significantly elevated S100A2 expression in the DFU group compared with that in the DFS group ($P < 0.05$). S100A2 exhibited consistently high expression in the DFU group across both bulk RNA-seq datasets and DEGs in our own sample data. This finding aligns with qRT-PCR validation, thereby enhancing the robustness and credibility of our conclusions.

Therapeutic Drug Prediction

Based on the CAMP database results, 10 potential drugs for DFU were identified: SB-221284, gabazine, ruxolitinib, calyculin, zacopride, palonosetron, leflunomide, epibatidine, tracazolate, and zardaverine. These agents were predicted to interact with immune hub genes (Table 1), among which ruxolitinib and leflunomide are commonly used clinically.

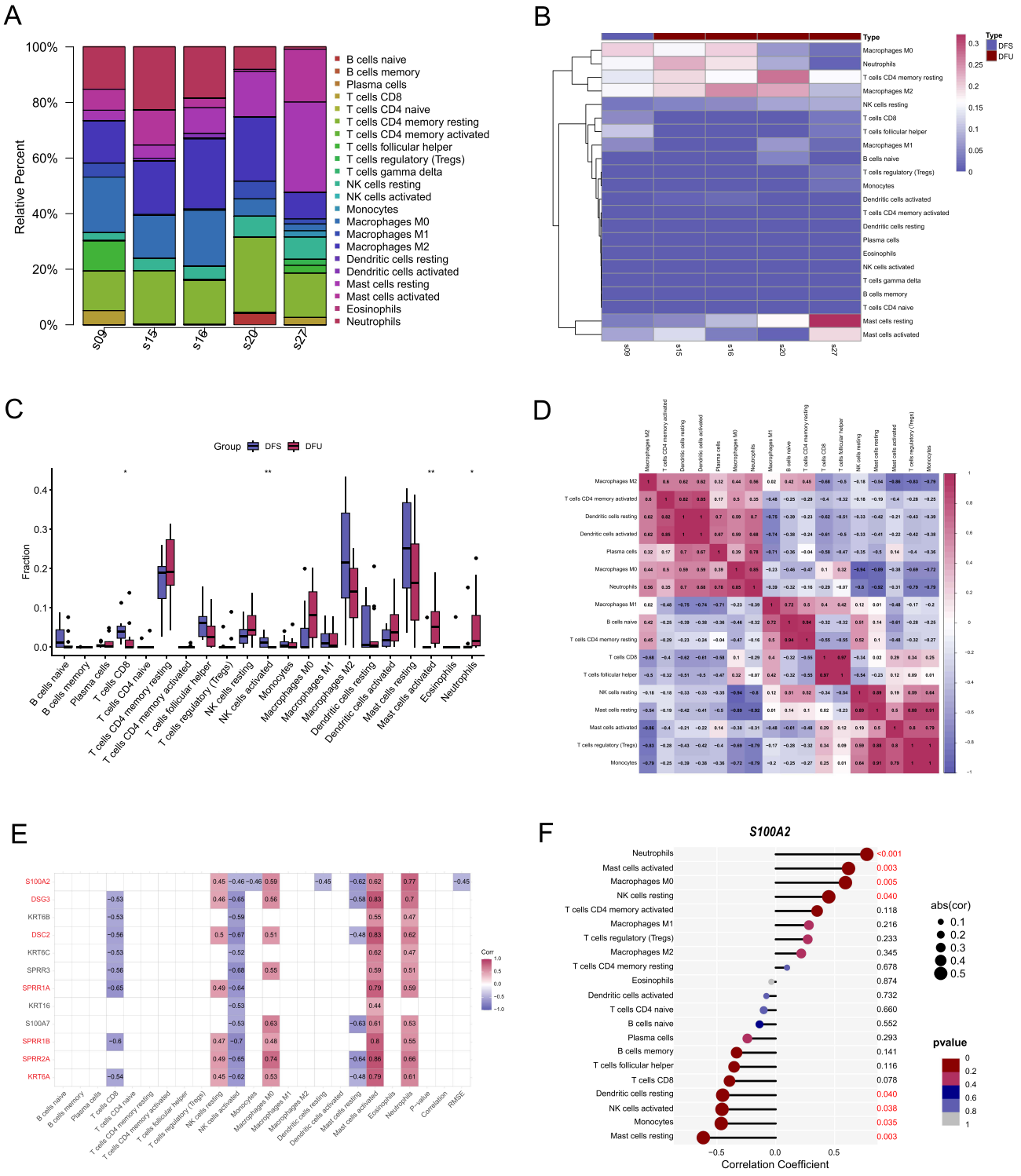

Figure 6 Immune infiltration profiling in the GSE134431. (**A**) Bar plot indicates the proportion of 22 immune cells. (**B**) Heat map indicates the abundance of 22 immune cells. (**C**) Differential expression of immune cells between DFU and DFS. **P* < *0.05*, ***P* < *0.01*, ****P* < *0.001*. (**D**) Correlation heat map of immune cells. (**E**) Correlation map between hub genes and immune features. Immune key genes were selected based on criteria: correlation coefficient > 0.7 and *P* < *0.05*. (**F**) Lollipop plot of S100A2.

Discussion

By integrating bulk RNA-seq and ScRNA-seq, we systematically investigated the composition of the immune hub genes and immunocytes in DFU. Therapeutic drugs for DFU have been identified. Our findings revealed a novel association between DFU pathogenesis and the IL-17 signaling pathway, which is a critical modulator of inflammatory processes.

https://doi.org/10.2147/JIR.S577432

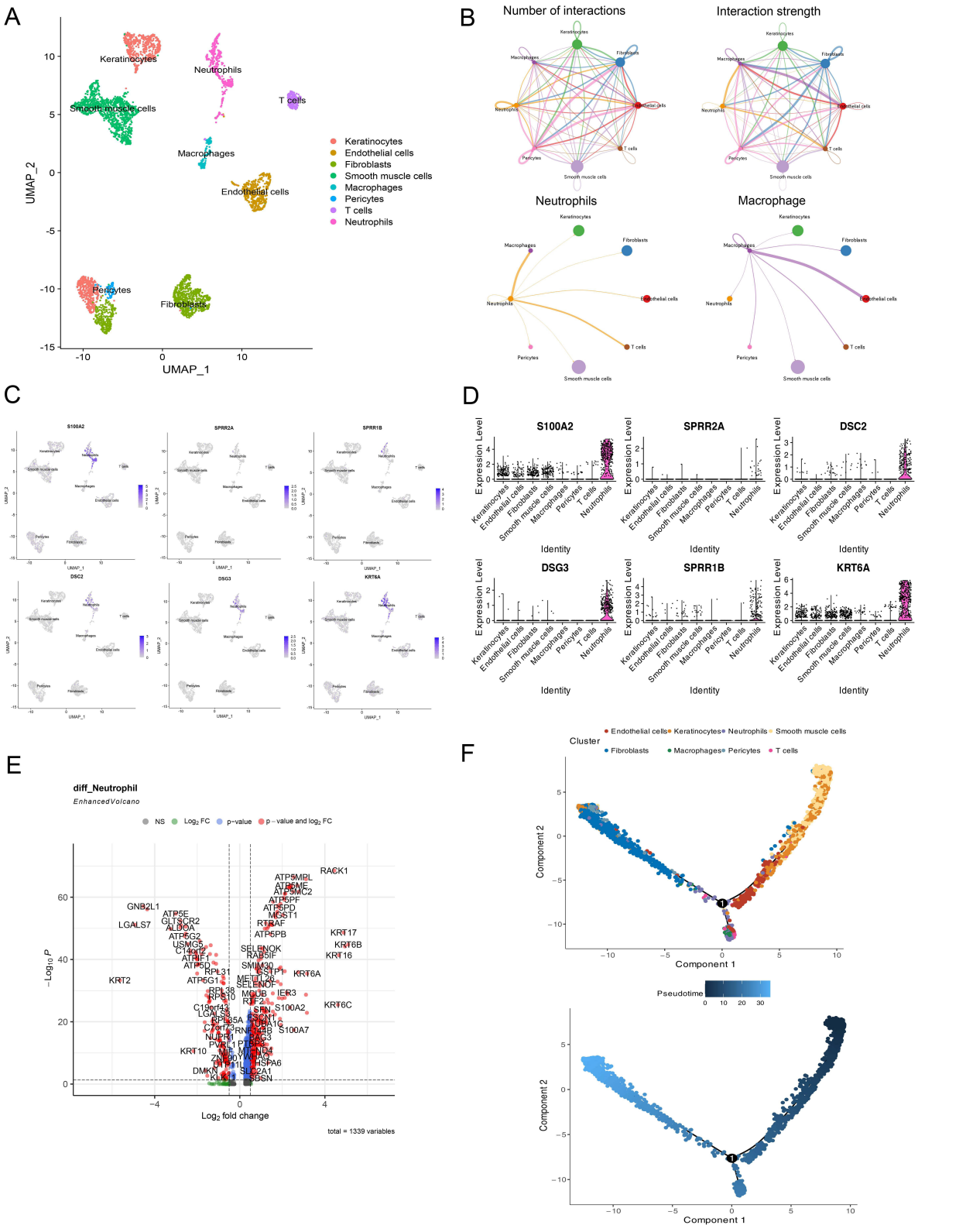

Figure 7 Sc RNA-seq analysis of the DFU. (**A**) UMAP plot of 8 cell clusters. (**B**) Quantification of interactions frequency and strength between 8 cells. (**C**) UMAP plots of six immune hub genes in each cluster. (**D**) Violin plots of six immune hub genes across clusters. Among these immune key genes, S100A2 is the characteristic gene of neutrophils. (**E**) Volcano plot of DEGs in neutrophils between DFU and DFS. (**F**) Pseudotime differentiation trajectory. Color intensity represents the temporal order of differentiation. The darker color is the initiation of differentiation and the lighter color is the differentiation terminal.

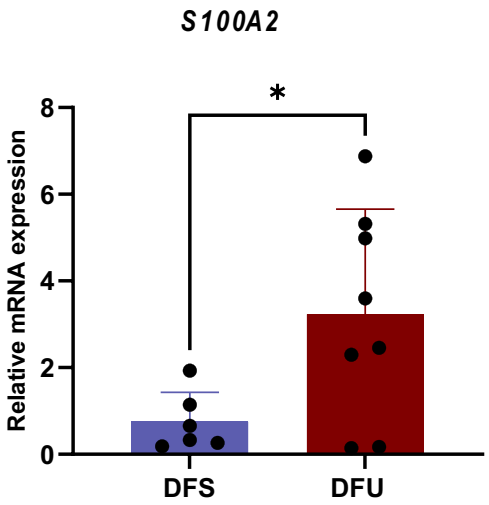

Figure 8 Relative expression level of S100A2 in DFS group and DFU group. *, $P < 0.05$. β-actin served as the housekeeping gene.

Wound healing is a complex process comprising four phases: hemostasis, inflammation, proliferation, and remodeling.[7] As the vanguard of the inflammatory response, neutrophils constitute the primary immune infiltrate post-injury, performing dual functions in microbial eradication and the activation of repair-associated cells.[18,19] Inflammatory cell infiltration during the initial phase of wound repair is dominated by neutrophils that execute pathogen clearance along with mononuclear phagocytes responsible for engulfing apoptotic neutrophils and reinitiating epithelial cell migration to achieve wound closure.[20,21] Consistently, the immune infiltration analysis in this study showed a significant neutrophilic predominance in DFU compared with DFS. This indicates that neutrophils are characteristic immune cells that distinguish DFU from DFS, which can be further validated by scRNA-seq. Emerging research has emphasized bidirectional communication between fibroblasts and monocytes or macrophages in the pathophysiological settings of inflammation and cutaneous remodeling, implying mutual regulatory mechanisms.[22,23] Interestingly, in our scRNA-seq analysis, the intercellular crosstalk profile showed prominent interactions between neutrophils and macrophages, along with their extensive connections to fibroblasts, endothelial cells, and keratinocyte subsets. These interactions may form a core regulatory network that drives inflammatory persistence in DFU wounds. Notably, the pseudotime trajectory analysis revealed that neutrophils act as the starting population of cell state transitions, with subsequent differentiation toward three distinct directions. This pattern suggests that neutrophils, as key inflammatory cells in DFU,

Table 1 Hub Genes Was Used to Predict Potential Drugs for the Treatment of DFUs. The Negative Sign Means That the Drug Antagonizes DFUs, and the Larger the Absolute Value, the Better the Treatment Effect

Name	Score	Description
SB-221284	−99.93	Serotonin receptor antagonist
Gabazine	−99.93	GABA receptor antagonist
Ruxolitinib	−99.89	JAK inhibitor
Calyculin	−99.89	Protein phosphatase inhibitor
Zacopride	−99.86	Serotonin receptor antagonist
Palonosetron	−99.82	Serotonin receptor antagonist
Leflunomide	−99.82	Dihydroorotate dehydrogenase inhibitor
Epibatidine	−99.82	Acetylcholine receptor agonist
Tracazolate	−99.74	GABA receptor modulator
Zardaverine	−99.68	Phosphodiesterase inhibitor

https://doi.org/10.2147/JIR.S577432

may undergo dynamic state changes to participate in different biological processes (eg., inflammatory response, tissue remodeling) during wound progression.

Through the integration of DEGs, WGCNA, immune infiltration analysis, and scRNA-seq analysis, S100A2 was recognized as the immune hub gene of DFU as well as the characteristic gene of neutrophils. S100A2 belongs to the S100 protein family of EF-hand calcium-binding proteins, which are primarily expressed and secreted by granulocytes such as neutrophils.[24] S100A family members are extensively involved in the regulatory processes of diverse inflammatory diseases, such as ischemic myocarditis, psoriasis, uveitis, and chorioamnionitis,[13,25–27] however, there are few reports on the association between S100A and DFU. During the early inflammatory phase, interleukin-1α (IL-1α), interleukin-33 (IL-33), and S100A family members interact synergistically to regulate inflammatory cascades and danger-signal activation.[28,29] S100A2 regulates keratinocyte differentiation, proliferation and wound healing.[30] Mechanistically, our findings demonstrate that neutrophils can promote the progression of DFU through S100A2. Additionally, Chen et al demonstrated that elevated S100A2 expression is associated with the remodeling of the tumor immune microenvironment, characterized by augmented IL-17 and tumor necrosis factor (TNF) signaling cascades, along with attenuated adaptive immune responses.[31] Yu et al also reported that S100A2 may contribute to the progression of schizophrenia through the IL-17 signaling pathway.[32] IL-17, a crucial pro-inflammatory cytokine produced by helper T cells (Th17) and innate immune effector cells,[33,34] mediates the pathological processes of various inflammatory reactions and autoimmune disorders. The IL-17 receptor (IL-17R) transduces signals via the Act1-TRAF6 complex, activating canonical pathways, such as NF-κB and JNK,[35] which drive pro-inflammatory gene expression and contribute to disease progression in conditions ranging from rheumatoid arthritis to psoriasis. This study implicated dysregulated IL-17 signaling in DFU pathogenesis, thus uncovering a previously unrecognized therapeutic target. Consistent with our findings that the IL-17 signaling pathway mediates DFU progression via S100A2 in neutrophils, we once reported that interleukin-37 (IL-37), a natural suppressor of innate inflammation, accelerates wound healing in diabetic mice by inhibiting the MAPK/NLRP3 pathway.[36] Their study demonstrated that suppression of proinflammatory cytokines and attenuation of macrophage infiltration are critical for resolving the persistent inflammatory microenvironment in DFU, which aligns with our observation that targeting neutrophil-associated inflammatory cascades could be a promising therapeutic direction. Together, these findings collectively support the notion that modulating dysregulated inflammatory pathways, whether IL-17, MAPK/NLRP3, or other interconnected axes, represents a core strategy for improving DFU outcomes. S100A2 in epithelial cells inhibits cutaneous wound repair by augmenting p53-mediated signaling in epidermal keratinocytes, thereby impeding the re-epithelialization process that is essential for epidermal regeneration after injury.[30] Yoshioka et al proposed S100A2 as a plausible biomarker for keratinocyte injury in various inflammatory skin conditions.[37] Our results further support an association between DFU and keratinocyte dysfunction, warranting further research.

Drug discovery involves identification of clinically actionable compounds from existing molecular databases. Secukinumab, a high-affinity monoclonal antibody targeting IL-17A, neutralizes its activity and is clinically approved for the treatment of psoriasis and ankylosing spondylitis treatment.[38,39] Given our mechanistic insights, secukinumab is a promising candidate for DFU treatment via the targeted inhibition of the IL-17 pathway. Furthermore, our computational screening identified ten agents, among which ruxolitinib and leflunomide are commonly employed in clinical practice.

Our core findings on S100A2 as a neutrophil-specific biomarker and its association with the IL-17 signaling pathway are strongly supported by integrated multi-omics analyses and qRT-PCR validation in clinical samples. Several inherent limitations of this investigation should be noted. First, regarding mechanistic validation, while we identified the S100A2-IL-17 axis via multi-omics, we did not perform downstream experiments (eg., Co-IP or Western Blot) to confirm the direct molecular interaction between S100A2 and the IL-17 receptor, nor did we assess the phosphorylation status of downstream effectors like NF-κB or JNK in our clinical samples. Second, the therapeutic potential of predicted drugs, particularly secukinumab, relies on bioinformatic inference. Although secukinumab is clinically validated for IL-17-mediated psoriatic inflammation, its specific efficacy in promoting DFU wound healing and suppressing neutrophil infiltration requires verification in diabetic animal models. Third, our clinical validation cohort was relatively small and lacked stratification by wound chronicity or vascular comorbidities. Future studies with larger, stratified cohorts and

rigorous functional assays like S100A2 knockdown in vivo are essential to solidify these findings and translate them into clinical practice. Transitional studies using animal models and clinical trials are essential to advance these findings for clinical applications.

Conclusions

Collectively, this exploratory bioinformatics study (integrating bulk and single-cell RNA-seq) elucidates S100A2 as a neutrophil-specific immune hub gene that mediates DFU pathogenesis through the IL-17 signaling pathway. Neutrophil-driven inflammation and immune dysregulation are critical for DFU progression, providing a novel diagnostic biomarker and potential therapeutic target. While secukinumab, ruxolitinib, and leflunomide are predicted to antagonize S100A2-IL-17 signaling, their clinical application for DFU requires further preclinical and clinical validation.

Data Sharing Statement

All datasets supporting this research are either publicly available or accessible to the corresponding author upon submitting a formal request.

Ethics Statement

The study protocol was approved by the Ethics Committee of the Huashan Hospital (KY2016-395) and complies with the Declaration of Helsinki. Before surgery, patients were comprehensively briefed on study participation and voluntarily signed consent forms. This study followed the RECORD guidelines.[40]

Author Contributions

Luqin Lv contributed to conceptualization, data curation, formal analysis, and writing – original draft. Yizhuo Zhang participated in data curation, formal analysis, visualization, and writing – original draft. Luqin Lv and Yizhuo Zhang contributed equally to this work. Qiaoli Cui was involved in investigation, validation and and writing – original draft. Xiaoming Zhu contributed to resources, conceptualization and writing – review and editing. Yijian Chen took charge of methodology, project administration, supervision, and writing – review and editing. All authors gave final approval of the version to be published; have agreed on the journal to which the article has been submitted; and agree to be accountable for all aspects of the work.

Funding

This work was supported by the Multidisciplinary Diagnosis and Treatment (MDT) Construction Project of Diabetic Foot (No:3030294002) and by grants from the (MDT) demonstration project in research hospitals (Shanghai Medical College, Fudan University, No: DGF501069/015).

Disclosure

The authors declare that they have no conflicts of interest in this study.

References

1. WHO. Diabetes. Available from: http://www.who.int/diabetes/en/. Accessed Sept 22, 2023.
2. Singh N, Armstrong DG, Lipsky BA. Preventing foot ulcers in patients with diabetes. *JAMA*. 2005;293(2):217–228. doi:10.1001/jama.293.2.217
3. Zhang Y, Lazzarini PA, McPhail SM, van Netten JJ, Armstrong DG, Pacella RE. Global Disability Burdens of Diabetes-Related Lower-Extremity Complications in 1990 and 2016. *Diabetes Care*. 2020;43(5):964–974. doi:10.2337/dc19-1614
4. Pickwell K, Siersma V, Kars M, et al. Predictors of lower-extremity amputation in patients with an infected diabetic foot ulcer. *Diabetes Care*. 2015;38(5):852–857. doi:10.2337/dc14-1598
5. Rice JB, Desai U, Cummings AK, Birnbaum HG, Skornicki M, Parsons NB. Burden of diabetic foot ulcers for medicare and private insurers. *Diabetes Care*. 2014;37(3):651–658. doi:10.2337/dc13-2176
6. Aumiller WD, Dollahite HA. Pathogenesis and management of diabetic foot ulcers. *JAAPA*. 2015;28(5):28–34. doi:10.1097/01.JAA.0000464276.44117.b1
7. Okonkwo UA, DiPietro LA. Diabetes and Wound Angiogenesis. *Int J Mol Sci*. 2017;18(7). doi:10.3390/ijms18071419
8. Yang Q, Cao J, Mi B, et al. Research Status and Development Trend of Mechanisms Underlying Diabetic Foot in China and Aboard Based on Bibliometrics. *World J Integrat Traditional Western Med*. 2023;18(09):1697–1704+1710. doi:10.13935/j.cnki.sjzx.230901

9. Schaper NC, Van Netten JJ, Apelqvist J, et al. Practical Guidelines on the prevention and management of diabetic foot disease (IWGDF 2019 update). *Diabetes Metab Res Rev*. 2020;36(1):e3266. doi:10.1002/dmrr.3266
10. Lim JZM, Ng NSL, Thomas C. Prevention and treatment of diabetic foot ulcers. *J R Soc Med*. 2017;110(3):104–109. doi:10.1177/0141076816688346
11. Theocharidis G, Thomas BE, Sarkar D, et al. Single cell transcriptomic landscape of diabetic foot ulcers. *Nat Commun*. 2022;13(1):181. doi:10.1038/s41467-021-27801-8
12. Schafer BW, Heizmann CW. The S100 family of EF-hand calcium-binding proteins: functions and pathology. *Trends Biochem Sci*. 1996;21(4):134–140. doi:10.1016/s0968-0004(96)80167-8
13. Liang H, Li J, Zhang K. Pathogenic role of S100 proteins in psoriasis. *Front Immunol*. 2023;14:1191645. doi:10.3389/fimmu.2023.1191645
14. Hurlow JJ, Humphreys GJ, Bowling FL, McBain AJ. Diabetic foot infection: a critical complication. *Int Wound J*. 2018;15(5):814–821. doi:10.1111/iwj.12932
15. Ramirez HA, Pastar I, Jozic I, et al. Staphylococcus aureus Triggers Induction of miR-15B-5P to Diminish DNA Repair and Deregulate Inflammatory Response in Diabetic Foot Ulcers. *J Invest Dermatol*. 2018;138(5):1187–1196. doi:10.1016/j.jid.2017.11.038
16. Sawaya AP, Stone RC, Brooks SR, et al. Deregulated immune cell recruitment orchestrated by FOXM1 impairs human diabetic wound healing. *Nat Commun*. 2020;11(1):4678. doi:10.1038/s41467-020-18276-0
17. Subramanian A, Narayan R, Corsello SM, et al. A Next Generation Connectivity Map: L1000 Platform and the First 1,000,000 Profiles. *Cell*. 2017;171(6):1437–1452e1417. doi:10.1016/j.cell.2017.10.049
18. Martin P, Leibovich SJ. Inflammatory cells during wound, repair: the good, the bad and the ugly. *Trends Cell Biol*. 2005;15(11):599–607. doi:10.1016/j.tcb.2005.09.002
19. Brinkmann V, Reichard U, Goosmann C, et al. Neutrophil extracellular traps kill bacteria. *Science*. 2004;303(5663):1532–1535. doi:10.1126/science.1092385
20. Wilgus TA, Roy S, McDaniel JC. Neutrophils and Wound Repair: positive Actions and Negative Reactions. *Adv Wound Care*. 2013;2(7):379–388. doi:10.1089/wound.2012.0383
21. Eming SA, Krieg T, Davidson JM. Inflammation in wound repair: molecular and cellular mechanisms. *J Invest Dermatol*. 2007;127(3):514–525. doi:10.1038/sj.jid.5700701
22. Humeres C, Vivar R, Boza P, et al. Cardiac fibroblast cytokine profiles induced by proinflammatory or profibrotic stimuli promote monocyte recruitment and modulate macrophage M1/M2 balance in vitro. *J Mol Cell Cardiol*. 2016. doi:10.1016/j.yjmcc.2016.10.014
23. Ploeger DT, Hosper NA, Schipper M, Koerts JA, de Rond S, Bank RA. Cell plasticity in wound healing: paracrine factors of M1/ M2 polarized macrophages influence the phenotypical state of dermal fibroblasts. *Cell Commun Signal*. 2013;11(1):29. doi:10.1186/1478-811X-11-29
24. Carvalho A, Lu J, Francis JD, et al. S100A12 in Digestive Diseases and Health: a Scoping Review. *Gastroenterol Res Pract*. 2020;2020:2868373. doi:10.1155/2020/2868373
25. Rohde D, Schön C, Boerries M, et al. S100A1 is released from ischemic cardiomyocytes and signals myocardial damage via Toll-like receptor 4. *EMBO Mol Med*. 2014;6(6):778–794. doi:10.15252/emmm.201303498
26. Golubinskaya V, Puttonen H, Fyhr IM, et al. Expression of S100A Alarmins in Cord Blood Monocytes Is Highly Associated With Chorioamnionitis and Fetal Inflammation in Preterm Infants. *Front Immunol*. 2020;11:1194. doi:10.3389/fimmu.2020.01194
27. Tong L, Lan W, Lim RR, Chaurasia SS. S100A proteins as molecular targets in the ocular surface inflammatory diseases. *Ocul Surf*. 2014;12(1):23–31. doi:10.1016/j.jtos.2013.10.001
28. Holzinger D, Tenbrock K, Roth J. Alarmins of the S100-Family in Juvenile Autoimmune and Auto-Inflammatory Diseases. *Front Immunol*. 2019;10:182. doi:10.3389/fimmu.2019.00182
29. Donato R, Cannon BR, Sorci G, et al. Functions of S100 proteins. *Curr Mol Med*. 2013;13(1):24–57.
30. Pan SC, Li CY, Kuo CY, et al. The p53-S100A2 Positive Feedback Loop Negatively Regulates Epithelialization in Cutaneous Wound Healing. *Sci Rep*. 2018;8(1):5458. doi:10.1038/s41598-018-23697-5
31. Chen Y, Wang C, Song J, Xu R, Ruze R, Zhao Y. S100A2 is a Prognostic Biomarker Involved in Immune Infiltration and Predict Immunotherapy Response in Pancreatic Cancer. *Front Immunol*. 2021;12:758004. doi:10.3389/fimmu.2021.758004
32. Yu S, Qu Y, Du Z, et al. The expression of immune related genes and potential regulatory mechanisms in schizophrenia. *Schizophr Res*. 2023. doi:10.1016/j.schres.2023.11.007
33. Korn T, Bettelli E, Oukka M, Kuchroo VK. IL-17 and Th17 Cells. *Annu Rev Immunol*. 2009;27:485–517. doi:10.1146/annurev.immunol.021908.132710
34. Cua DJ, Tato CM. Innate IL-17-producing cells: the sentinels of the immune system. *Nat Rev Immunol*. 2010;10(7):479–489. doi:10.1038/nri2800
35. Qu F, Gao H, Zhu S, et al. TRAF6-dependent Act1 phosphorylation by the IkappaB kinase-related kinases suppresses interleukin-17-induced NF-kappaB activation. *Mol Cell Biol*. 2012;32(19):3925–3937. doi:10.1128/MCB.00268-12
36. Cui Q, Zhang Z, Qin L, et al. Interleukin-37 promotes wound healing in diabetic mice by inhibiting the MAPK/NLRP3 pathway. *J Diabetes Investig*. 2025;16(3):405–413. doi:10.1111/jdi.14389
37. Yoshioka M, Sawada Y, Saito-Sasaki N, et al. High S100A2 expression in keratinocytes in patients with drug eruption. *Sci Rep*. 2021;11(1):5493. doi:10.1038/s41598-021-85009-8
38. Langley RG, Elewski BE, Lebwohl M, et al. Secukinumab in plaque psoriasis--results of two Phase 3 trials. *New Engl J Med*. 2014;371(4):326–338. doi:10.1056/NEJMoa1314258
39. Blair HA. Secukinumab: a Review in Ankylosing Spondylitis. *Drugs*. 2019;79(4):433–443. doi:10.1007/s40265-019-01075-3
40. Data RosCuOR-c. What is RECORD? Available from: http://www.record-statement.org/. Accessed Dec 01, 2025.